Chemical Physics 398 (2012) 134–141

Contents lists available at ScienceDirect

Chemical Physics

journal homepage: www.elsevier.com/locate/chemphys

Lifetime and kinetic energy release of metastable dications dissociation

M. Alagia [a], P. Candori [b], S. Falcinelli [b], K.C. Mundim [c,d], M.S.P. Mundim [c,e], F. Pirani [c], R. Richter [f], S. Stranges [a,g], F. Vecchiocattivi [b,*]

[a] IOM CNR Laboratorio TASC, I-34012 Trieste, Italy
[b] Dipartimento di Ingegneria Civile ed Ambientale, 06125 Perugia, Italy
[c] Dipartimento di Chimica Università di Perugia, 06123 Perugia, Italy
[d] Instituto de Química, Universidade de Brasilia, Caixa Postal 4478, 70904-970 Brasilia, Brazil
[e] Instituto de Fisica, Universidade Federal da Bahia, 40000 Salvador, Brazil
[f] Sincrotrone Trieste, Area Science Park, 34149 Basovizza, Trieste, Italy
[g] Dipartimento di Chimica, Università di Roma "La Sapienza", 00185 Roma, Italy

ARTICLE INFO

Article history:
Available online 8 April 2011

Keywords:
Double photoionization
Statistical methods

ABSTRACT

A new method for the determination of dynamical features of the molecular dication dissociation processes, following the single photon double ionization, investigated by time-of-flight mass spectrometry technique has been developed. The method is based on an extension of the generalized simulated annealing statistical methodology, previously applied in other fields. Here it is described and applied, as an example, to the case of the dissociation of the CO_2^{2+} dication giving $CO^+ + O^+$ ion fragments. The results are consistent with previous determination of the metastable lifetime of the dication, but the analysis also provides additional information about the dynamics of the reaction.

1. Introduction

The physical and chemical properties of molecular dications are rather different from those of both singly charged ions and neutral molecules. In solution dications can be stabilized by solvent interactions, however, in the gas phase they are unstable in most cases. This is due to the coulombic repulsion between the two charges that can produce a dissociation of the molecular dication in two singly charged ions. Moreover, in some cases the couplings by charge transfer effects can produce the formation of a metastable state [1–5]. It follows that the dynamics and the lifetimes of these doubly charged metastable states can selectively affect several microscopic and macroscopic phenomena.

These doubly charged species have an important role in plasma chemistry and physics: a plasma may contain many molecular ions, and under some conditions molecular dications are present in significant concentrations. Molecular dications are also present in the ionosphere [6] of the earth or of other planets and are of interest in interstellar clouds and in hot material surrounding star forming regions [7].

Theoretical calculations of the properties of molecular dications are far more difficult than similar calculations for neutral molecules or singly charged ions with equivalent numbers of electrons and nuclear masses. In fact, computing the properties of molecular dications typically requires full configuration interaction calculations using very large basis sets.

The simplest mechanisms by which gas phase molecular dications can be produced are electron impact ionization, or double-photo-ionization. Synchrotron radiation provides the possibility of studying the double-photo-ionization of molecules by a single photon, with high intensity light, allowing the observation of rather detailed features of the spectroscopy and dynamics of the parent ion and its fragments.

In recent years, we have investigated the double photo-ionization of some simple molecules, like HCl [3,8], HBr [5,9], HI [10], N_2O [11,12], CO_2 [13,14], and benzene [15]. For these systems, the double ionization has been studied as a function of the photon energy, by measuring the ion products with time-of-flight mass spectrometry and, in the case of charge separation processes, by detecting in coincidence the two fragment ions. For HBr, we have also measured in coincidence the two threshold photoelectrons [16], obtaining interesting information about the low lying electronic and vibrational states of the molecular dication.

The typical experimental scheme for measuring photoelectron–photoion–photoion coincidences is sketched in Fig. 1. The photo-ionization events occur in the scattering volumes, where the ultraviolet synchrotron light crosses the molecular beam formed of ABC molecules. The grids g_1 and g_2 establish an electric field that sends the photoelectron towards the electron detector and the ions in the opposite direction. The latter are then extracted and, after acceleration due to the field of grid g_3, enter into the drift

* Corresponding author. Tel.: +39 0755853862; fax: +39 0755853864.
E-mail address: vecchio@dyn.unipg.it (F. Vecchiocattivi).

0301-0104/$ - see front matter © 2011 Elsevier B.V. All rights reserved.
doi:10.1016/j.chemphys.2011.03.031

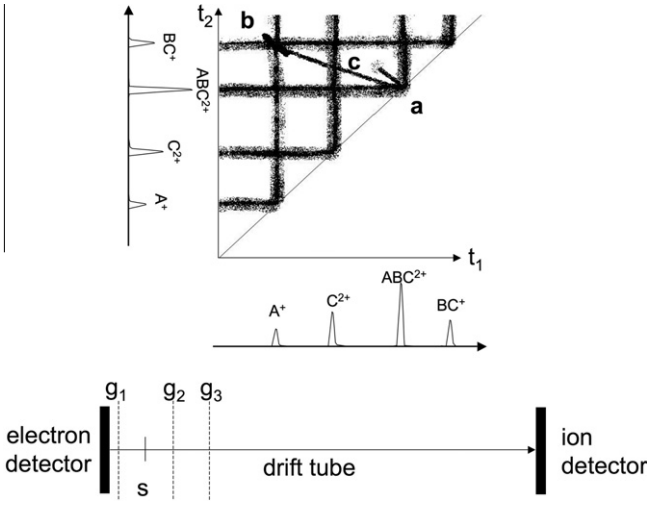

Fig. 1. In the lower part shows the schematics of a typical time-of-flight mass spectrometer. Ions are formed by photoionization in the location **s**, inside the grid system g_1, g_2 and g_3. In the upper part, a typical coincidence plot for the double photoionization of a molecule ABC is shown. In the plot, the t_1 and t_2 time-of-flight values for ions produced in coincidence with the same electron are reported as points. The photoion peaks are represented by horizontal and vertical ribbons of high intensity points. The location **a** is where ABC^{2+} dication are recorded, while the spot in **b** represents A^+ and BC^+ ions in coincidence, i.e. produced in the same ionization event. The tail **c**, connecting the locations **a** and **b**, represents pairs of ions produced by the same dication, after a dissociation occurring along the path from **s** to the ion detector. Therefore we can say that in **a** stable dications, in **b** pairs of ions produced by instantaneous dissociations, and in **c** pairs of ions from metastable dications are recorded.

tube where they fly to the ion detector. The pulses generated by the ions arriving at the detector are recorded as a function of the delay time with respect to the photoelectron. The typical results of a photoelectron–photoion–photoion-coincidence measurement, in the dissociative ion–ion formation reaction following the double photoionization of molecule, are usually reported in an ion–ion coincidence plot, also shown schematically in the upper part of Fig. 1. In such a plot one reports the delay time between the pairs of ions arriving at the detector correlated with the same photoelectron. The vertical and horizontal ribbons, due to high density of points, indicate the ions correlated with the start pulse of the photoelectron. The position **a** refers to the signal produced by the molecular ABC^{2+} dication, while the spot in the position **b** indicates the $t_1 - t_2$ region for the observation of A^+/BC^+ coincidences, in other words ions correlated with the same photoelectron. The tail **c** connecting positions **a** and **b**, represents pairs of ions produced by the ABC^{2+} dication dissociating into $A^+ + BC^+$ along the drift tube. Considering the time scale, we can assert that ions dissociating during a very short time, given by the difference between the t_1 and t_2 limits in the spot **b**, are enclosed in that spot. Dications with a lifetime longer than the characteristic ion flight time along the drift tube are detected in the position **a**. The ions detected along the tail are those produced by metastable dications with a lifetime comparable to the dication flight time along the drift tube. It is important to stress that the characteristic times for the definition of an instantaneous dissociation, the metastability of the dication, or the formation of a stable doubly charged ion, are depending on the geometrical characteristics of the experimental device and on the applied electrical potentials. These conditions also determine the time resolution of the experiment.

In order to better describe the matter reported above, we discuss the results of two real experiments. In Fig. 2 the plot of coincidences, as measured for the double photoionization of CO_2 at 44 eV photon energy, is reported [13,14]. The formation of a stable

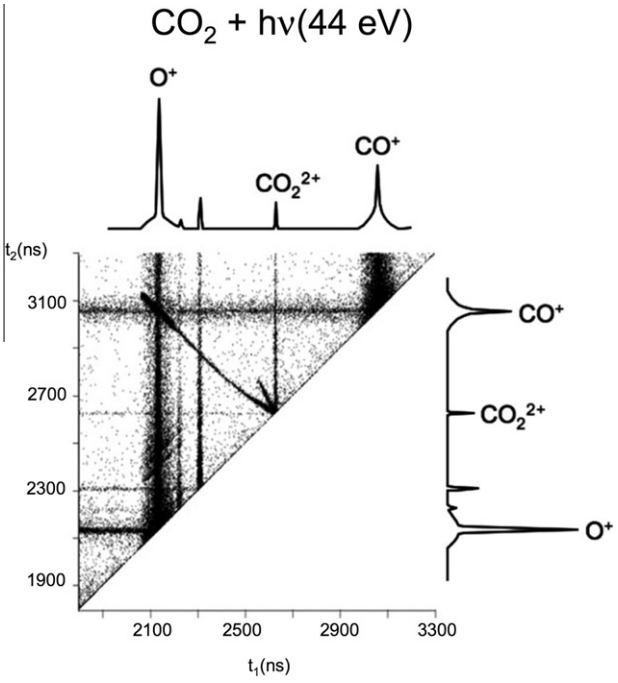

Fig. 2. Ion coincidence plot of the double photoionization of CO_2 as measured at 44 eV photon energy (see Fig. 1 and text).

CO_2^{2+} dication is quite evident, as well as the instantaneous dissociation into O^+ and CO^+, but also the same dissociation via a metastable dication. From the size of the O^+/CO^+ coincidence spot we can define that the instrument (described below) recognizes as instantaneous dissociations those occurring in a time shorter than 50 ns, while the dications seen as stable are those living for a time longer than 2.5 μs. Therefore, dissociations occurring via metastable dication states must happen in the times interval between 50 ns and 2.5 μs. In Fig. 3 the plot of coincidences, as measured for the double photoionization of N_2O at the photon energy of

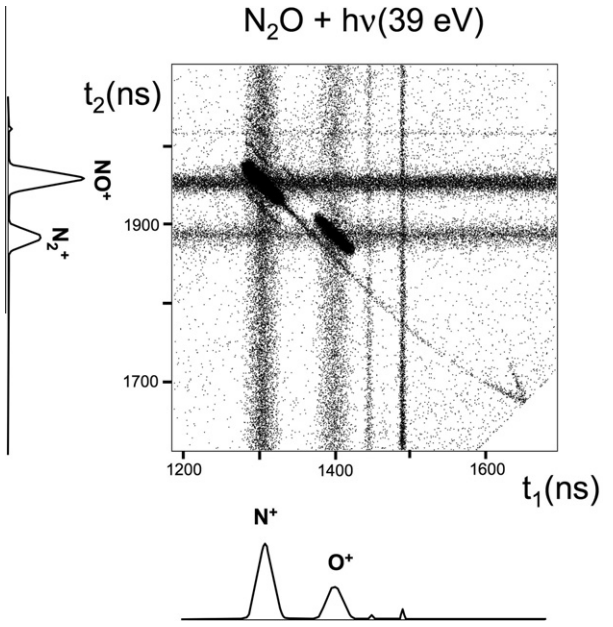

Fig. 3. Ion coincidence plot for the double photoionization of N_2O recorded at 39 eV photon energy (see Fig. 1 and text).

39 eV, is shown [11,12]. In this case, we observe two instantaneous charge separation channels, one leading to the formation of N_2^+ and O^+, while another produces NO^+ and N^+. For the latter it is evident that also dissociation via a metastable dication occurs, but a stable N_2O^{2+} dication is not formed.

From the two examples described above it emerges that the coincidence plots contain detailed qualitative information about the dynamics of processes promoted by the double photoionization of molecules. In order to extract also quantitative information a numerical analysis of the distribution of coincidences is necessary. In previous experiments a procedure, based on approximated expressions, obtained from a previous kinematical analysis [17], has been exploited by Field and Eland [18]. In other cases, a Monte Carlo trajectory simulation of the ion flight inside the instrument has been used [13,18,19]. We have used both methods [13], obtaining consistent results for the lifetime of the metastable dication and the kinetic energy release (KER) into the two product ions.

The extension and generalization of those methods to other systems appear somewhat difficult, especially because their mathematical basis has never been explicitly published and therefore the application to data obtained under different conditions is not immediate. In this paper we report on a new general stochastic method for the analysis of coincidence plots in order to extract details of the dynamics of charge separation processes of the type described above, especially for obtaining the relevant lifetimes. Such an analysis includes the definition of the geometry and the relevant electric fields in the time of flight mass spectrometer. In the next section the instrument used in our experiments is described in order to define conditions and parameters employed in the CO_2^{2+} and N_2O^{2+} experiments. Then the new method is illustrated in a following section, together with the algorithms used for the analysis. In the final section the results of its application are reported and discussed.

2. Description of the instrument

The apparatus exploited to obtain the coincidence plots of the type in Figs. 2 and 3 is operating at the synchrotron light laboratory ELETTRA (Trieste, Italy), in the ARPES end station of the Gasphase Beamline. Details about the beamline and the end station have been previously reported [11–14]. Only a brief description is given below (see Fig. 4).

The energy selected synchrotron light beam crosses an effusive molecular beam of target molecules. In most cases, this target gas is mixed with a rare gas employed for calibration reference measurements. The product ions are detected in coincidence with photoelectrons. The photon energy resolution provided by the monochromator is between 1.5 and 2.0 meV in the energy range recently investigated (25–55 eV). In order to avoid spurious effects due to the ionization by higher-order diffraction photons, a magnesium film filter is placed along the synchrotron radiation beam path. The molecular beam, the light direction and the ion detection axes are mutually perpendicular. The ion detection system has been assembled following the design described by Lavollèe [20]. Such a time-of-flight spectrometer, with an ion position sensitive detector, is designed specifically to measure the spatial momentum components of the dissociation ion products. The electron detector, located just below the interaction volume, consists of a stack of three micro-channel-plates followed by a copper anode. The ion detector also consists of a stack of three-micro-channel plates located at the end of a drift tube. The signals are read by an array of anodes arranged in 32 rows and 32 columns. Such an arrangement allows the detection of the ion arrival position on the detector plate. In our experiments the photoelectron signals are used as start pulses, and then ions are counted as a function

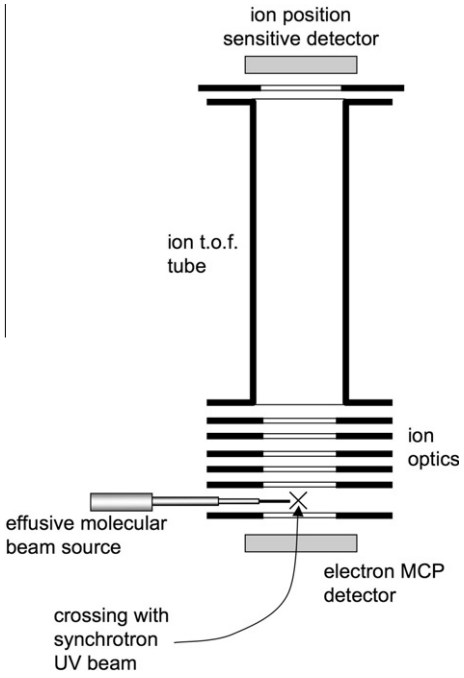

Fig. 4. A schematic representation of the instrument used for collecting the data shown in Figs. 2 and 3.

of their arrival time and position on the detector. All experiment components are controlled by a computer that also records experimental data.

As already mentioned above, the target gas is supplied to a needle beam source kept at room temperature, where it is also mixed with helium or argon. This allows us to normalize all ion signals, at each photon energy, to the total ion yield of the rare gas signal measured at that energy. An adjustable leak valve along the gas inlet line is used to control the gas flow, which is monitored by recording the pressure in the main vacuum chamber. The incident photon flux and the gas pressure are monitored and stored in separate acquisition channels. Ion yields are then corrected for pressure and photon flux changes while varying the photon energy.

3. The TOFMS-GSA method

In this paper we present and apply a new method to obtain a global optimization of an objective function, defined as chi-square between experimental and theoretical data. This method exploits an extension of the temperature concept, used to define the width of the distribution function of each physical variable. In the present case the temperature is permitted to vary to reach the lowest value, defining the most probable distribution of the examined variable. When the objective function represents the energy, the temperature concept assumes the thermodynamic meaning, while in other cases corresponds to a measure of the external noise. Therefore, the present method contains the Monte Carlo procedure, often exploited in the analysis of experimental data, as particular case where the temperature is maintained constant.

The Time-of-Flight Mass Spectrometry Generalized Simulated Annealing (TOFMS-GSA) methodology, employed to characterize the metastability of dications by using experimental data obtained by TOFMS technique, is based on an *inverse problem* that can be formulated by mapping the model parameters on experimental data, through physical considerations. In our case the physical model consists of a set of charged particles moving under the influence of external electrostatic fields. Inverse problems are often

formulated in infinite dimensional spaces. However, limitations due to a finite number of measurements, and the practical considerations of recovering only a finite number of unknown parameters, may lead to the problems being recast in discrete form. In this case the inverse problem will typically be conditioned, but the regularization may be used to introduce mild assumptions about the solution and prevent *overfitting*. Many instances of regularized inverse problems can be interpreted as special cases of Bayesian inference.

In our procedure the inverse problem is formulated through an objective function f, defined in a multi-dimensional parameter space as follows:

$$f(E_{KER}, \tau, v_o, S_o, \theta) = \sum_{i=1}^{2} (t_{i_{exp}} - t_{i_{theo}})^2 + \Delta p_z^2 + \Delta E_T^2 \sim 0, \quad (1)$$

where E_{KER}, τ, v_o, S_o are the kinetic energy released, the dication time of flight, the initial velocity and position, respectively. θ is the fragmentation angle of the ion momenta with respect to the detector axis. On the right side of Eq. (1), the first term is the chi-square deviation between the experimental and theoretical time of flights for the two ionic fragments obtained by solving, stochastically, the classical motion equation through the GSA procedure. Δp_z^2 is the chi-square deviation of the z component of the linear momentum, that is parallel to the detector axis, while ΔE_T^2 is the total energy chi-square deviation. Δp_z^2 and ΔE_T^2 are constrains to ensure linear momentum and total energy conservation. The ΔE_T^2 term is taken into account only if the ejected electron energy is known. The parameters representative of the analyzed systems are obtained by using classical mechanics to describe trajectories and energy properties of ionic fragments and comparing predictions with measured time of flight mass spectrometry data. The TOFMS-GSA procedure consists in solving, stochastically, the Newton's equations in order to map the set of parameters E_{KER}, τ, v_o, S_o, θ that minimize the objective function f defined by Eq. (1).

The main purpose of TOFMS is to collect a population of ions (fragments) moving in the direction of the detector and having a distribution of masses (M_i), charge (q_i), kinetic energy and velocities, the latter being inversely proportional to $\sqrt{M_i/q_i}$. When the fragment ions, under the influence of an external electric field and starting from the rest at the same time, are accelerated in the detector direction, their times of flight, following the usual TOF model [21], at the detector will be distributed according to $\sqrt{M_i/q_i}$. As shown in Figs. 4 and 5, our TOF mass spectrometer consists (see Fig. 5) of two acceleration regions, 1 and 2, followed by one field free region, 3, and two small acceleration region, 4 and 5, up to the detector. The values of potentials and the dimensions of each region, as used in the CO_2 experiments, are also given in the figure.

The detailed analysis of the experimental TOF requires no more than Newtonian physics, as shown by the equations reported in the following. The positions S of the ith fragment (di- or mono-cation) in the sector n of the TOF tube is described by

$$S_{n_i} = S_{n-1_i} + v_{n-1_i}\Delta t_{n_i} + \frac{1}{2} a_{n_i} \Delta t_{n_i}^2, \quad (2)$$

where the time of flight difference is $\Delta t_{n_i} = \frac{-v_{n-1_i} + \sqrt{v_{n-1_i}^2 + 2\Delta S_{n_i} a_{n_i}}}{a_{n_i}}$ and the fragment velocity is $v_{n_i} = v_{n-1} + v_{KER_i} + a_{n_i}\Delta t_{n_i}$. The acceleration of the ith fragment, in sector n, due the electric field is $\frac{V_n - V_{n-1}}{dS_{n_i}}$, is given by

$$a_{n_i} = \frac{2 \times 1.60210^{-19}}{M_i \times 1.66010^{-27}} \frac{V_n - V_{n-1}}{dS_{n_i}}, \quad (3)$$

where $V_n - V_{n-1}$ and dS_{n_i} are respectively the electrical potential difference and the dimension of the nth sector. The velocity (z component) of the fragments, parallel to the detector axis, and due to the kinetic energy release (E_{KER}), is equal to

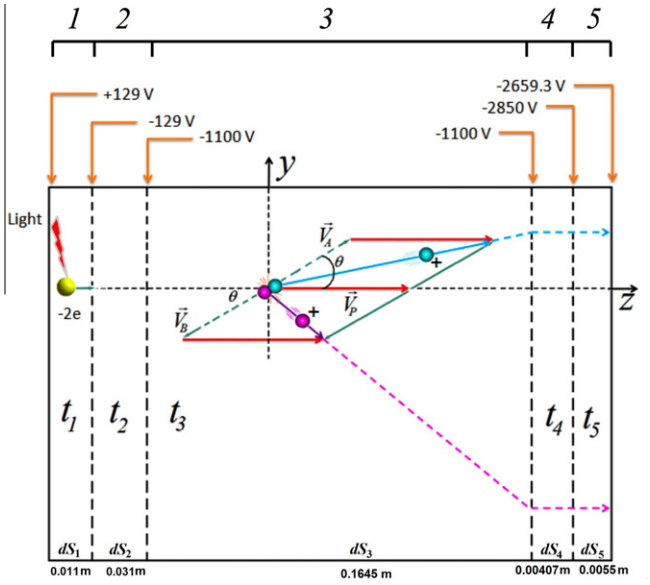

Fig. 5. Definition of the distances dS_i, the applied potentials and the time-of-flight t_i in the sectors i of the TOFMS instrument. The kinematic variables of ions are also indicated.

$$v_{z_{KER_A}} = \sqrt{\frac{E_{KER}}{M_A\left(1 + \frac{M_A}{M_B}\right)}} \cos(\theta), \quad (4)$$

$$v_{z_{KER_B}} = \sqrt{\frac{E_{KER}}{M_B\left(1 + \frac{M_B}{M_A}\right)}} \cos(\theta - \pi), \quad (5)$$

θ is the fragmentation angle in the TOF equipment diagram as shown in Fig. 5. The partial time of flight that the ith ion expends in each region n, is t_{i_n} and the total time $t_{i_{esime}}$ will be defined as

$$t_{i_{esime}} = \sum_{i=1}^{5} t_{in}. \quad (6)$$

4. Procedure of global optimization using the generalized simulated annealing

The global optimization problem is a subject of intense research and current scientific interest. Finding the optimal solution for a complex problem is of great importance in a variety of fields, such as image restoration, microprocessor circuitry design and protein folding [22] among others. In this context, we present an alternative methodology, based on the GSA global optimization method to analyze data from TOF experiments.

The simulated annealing (SA) corresponds to a stochastic method used in global procedures and it was proposed by Kirkpatrick and collaborators [23,24]. As stressed above, differently from the Monte Carlo and Metropolis methods [25], in SA the temperature T_{q_v} is time dependent and the "temperature" term used does not refer to the thermodynamic concept and the "time" is the number of cycle, n, in the GSA procedure. In this technique, the concept of artificial temperature is introduced and gradually cooled, in complete analogy with the well known annealing technique frequently used in metallurgy, when a molten metal reaches its crystalline state (global minimum of thermodynamic energy). In the literature, the SA algorithm is also referred to as classical simulated

annealing (CSA) and its visiting distribution, i.e. the procedure to map the range of variability of the parameter, is a Gaussian function, $g(\mathbf{x}) \propto e^{-\mathbf{x}^2/T_1(n)}/T_1(n)$. Geman and Geman [26] show that the necessary and sufficient condition for reaching convergence is that the temperature decreases logarithmically with time, that is $T_1(n) = T_0/\log(1+n)$, where T_0 is the initial temperature.

Szu and Hartley [27] propose to use a Cauchy–Lorentz visiting distribution function $g(\mathbf{x}) \propto T_2(n)/(T_2(n)^2 + \mathbf{x}^2)^{\frac{D+1}{2}}$, instead of a Gaussian one. D is the dimension of parameter space and, in our case, $D = 5$. This algorithm is referred to as fast simulated annealing (FSA) or Cauchy machine. In the reference [27] it is shown that, for a Cauchy–Lorentz visiting type of distribution function, the convergence procedure will reach a global minimum if temperature $T_2(n)$ decreases inversely with time, that is, $T_2(n) = T_0/(1+n)$. On the other hand, the GSA or Tsallis machine approach [28], which closely follows the recent statistical mechanics for non-extensive systems, has been proposed and applied in quantum chemistry [28,29]; GSA generalizes both the FSA and CSA procedures. So, as introduced in reference [28], instead of using a Gaussian or Cauchy–Lorentz visiting distribution function, the new one is defined as

$$g_{q_V}(x) = \frac{\left(\frac{q_V-1}{\pi}\right)^{D/2}\left[\Gamma\left(\frac{1}{q_V-1}+\frac{D-1}{2}\right)/\Gamma\left(\frac{1}{q_V-1}-\frac{1}{2}\right)\right]\left(\frac{\pi}{2}-\theta\right)\times[T_{q_V}(n)]^{\frac{D}{3-q_V}}}{\left\{1+\frac{(q_V-1)x^2}{[T_{q_V}(n)]^{\frac{2}{3-q_V}}}\right\}^{\frac{1}{q_V-1}+\frac{D-1}{2}}} \tag{7}$$

which has the following limits:

$$\begin{aligned}\lim_{q_V\to 1} g_{q_V}(x) &= g^{CSA}(x) = \frac{e^{\frac{x^2}{T_{q_T}(t)}}}{[\pi T_1(n)]^{D/2}},\\ \lim_{q_V\to 1} g_{q_V}(x) &= g^{FSA}(x) = \frac{\Gamma\left(\frac{D+1}{2}\right)}{\pi^{\frac{D+1}{2}}}\cdot\frac{T_2(n)}{[T_2(n)^2+x^2]^{\frac{D+1}{2}}},\end{aligned} \tag{8}$$

CSA and the FSA visiting distributions, respectively. The present approach defines the acceptance probability function as

$$A_{acc} = \left[1+(q_A-1)\frac{f(\vec{P}_{n+1})-f(\vec{P}_n)}{T_{q_T}(n)}\right]^{\frac{1}{1-q_A}} \tag{9}$$

which has the following limit if $q_A \to 1$

$$\lim_{q_A\to 1} A_{acc} = e^{\frac{[f(P_n)-f(P_{n-1})]}{T_{q_T}(n)}}. \tag{10}$$

The latter is the same acceptance probability function introduced in the CSA and FSA [27] procedures. In the usual GSA methodology, the new temperature is defined as

$$T_{q_V}(n) = T_0\frac{2^{q_V-1}-1}{(1+n)^{q_V-1}-1}. \tag{11}$$

Taking into account the limits $q_V \to 1$ and $q_V \to 2$ we obtain the temperature functions for the CSA and FSA procedures, respectively, as follows:

$$\begin{aligned}\lim_{q_V\to 1} T_{q_V}(n) &= T_1(n) = T_0\frac{\ln 2}{\ln(1+n)},\\ \lim_{q_V\to 2} T_{q_V}(n) &= T_2(n) = \frac{T_0}{n}.\end{aligned} \tag{12}$$

It has to be stressed again that the GSA approach has been used with success in predicting new three-dimensional protein structures and protein folding [22], in fitting the potential energy surface for reaction pathways and chemical reaction dynamics [30,31], gravimetric problems [32], mechanical properties in alloys [33,34] and the study of molecular electronic structure properties [35,36].

It has to be noted that in the previous equations q_V, q_A, q_T are parameters derived from the generalization of Boltzmann statistical mechanics. In particular, when $q_V = q_A = q_T = 1$ and T is constant, the method reduces to the Monte Carlo procedure.

When using the GSA procedure, proof of convergence to the absolute minimum can be obtained in the same way as was established by Szu and Hartley [27]. The TOFMS-GSA procedure, proposed here, starts with a given solution (combination of variables), then random changes are made in a typical "suck-it-and-see" approach. If an improvement is obtained, the old solution is always abandoned in favor of the new one. But if a worse result is obtained, the old solution may still be abandoned in the hope of getting a marked improvement after few steps. This check prevents the algorithm from being stuck in a local minimum, a state which has a value which larger than the global minimum, but smaller than any of its neighbors. However, the frequency with which this is done, decreases as time goes on (this is equivalent to gradually lowering the temperature), so that we should eventually end up at the global optimum, i.e. the best possible solution. While, to reach an acceptable solution could require a large number of trials, simulated annealing is extremely flexible in that rules can easily be devised to obtain new solutions of any kind, including those involving structural changes. More details on the methodology and on the presently suggested procedure are given in Appendix.

Another difference from traditional GSA is that we use a version exploiting in the algorithm also the q_T parameter, introduced in Ref. [36]. This makes the overall procedure more efficient, allowing convergence with a smaller number of cycles, when compared to the usual GSA process. However, when dealing with the traditional GSA algorithm, the proof of convergence to the absolute minimum, as established in the references [28,29], only includes the case of two independent q_A and q_V parameters. While, in the paper [36], by using a modified form of the distribution function, g_{q_V,q_T}, a proof of convergence was introduced for the absolute minimum, which is based on the alternative GSA [37] and defined with three independent parameters q_A, q_V and q_T.

5. Results and discussion

As a check of the procedure proposed in this paper, we have analyzed the CO_2 coincidence plot that has been already investigated with different methods [13]. In order to minimize the simulation computational time, we excluded the fragment time of flights or events, $t_1 \times t_2$, that are not first order correlated, which are usually contained in the experimental data. In the case of the CO_2 system, after the simulation, we have imposed that the chi-square deviation between experimental and theoretical ion time of flights and the linear momentum conservation, $\chi^2 = \sum_{i=1}^{2}(t_{i_{exp}} - t_{i_{theo}})^2 + (p_{A_z} - p_{B_z})^2$, must be $\chi^2 < 10^{-4}$ for each event. After the simulation and using the Newton's equation we have evaluated some physical features of the dissociation dynamics, like the kinetic energy release (KER), the fragmentation time, the position in the spectrometer or sector where the fragmentation occurs, the velocity of the dication and that of fragments and their angular orientation.

In Fig. 6 the experimental data (open circles) of the coincidence plot for the double photoionization of CO_2 at 44 eV, are reported and compared with the simulation results (black points). It is practically impossible to distinguish the two kinds of results, because the convergence of the simulation has been stopped when the chi-square deviation is really very small. As stressed above, from

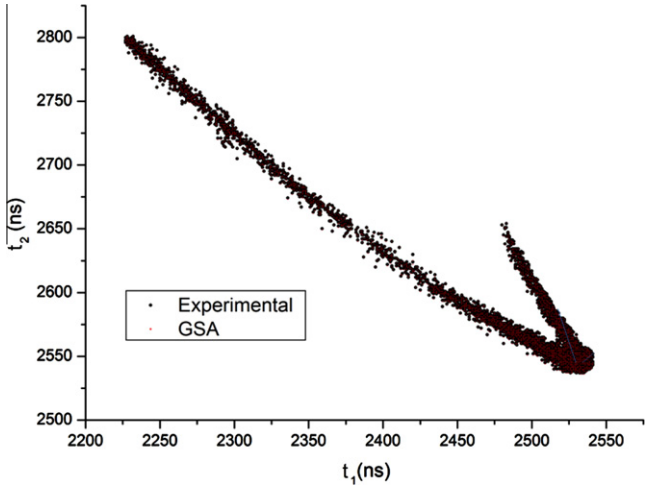

Fig. 6. Coincidence plot shown in Fig. 2, cleaned up of false coincidences and used for analysis. In the plot, the points produced by the simulation procedure are also reported (black points), but are overlapping the experimental dots (open circles) and therefore almost indistinguishable.

the analysis of the trajectories produced in the simulation, it is now possible to extract important dynamical features of the dissociation reaction under investigation. In Fig. 7 some of these features are plotted. In particular, the (a) panel reports the initial transversal velocity of the dication, at the beginning of the flight, while panel (b) gives the position where ions are produced by the VUV light; dications then fly up to the location, along the path, where dissociation occurs and panel (c) provides the distribution of such positions. In the panel (d) the KER in the dissociation, exhibiting a distribution around the most probable value, is reported, while in the (e) panel the angular distribution of the direction of the two ion products is displayed. The (f) panel shows the number of dications as a function of the flight time along the path in the drift tube. It is evident their decrease with time, caused by the dissociation reaction. This last distribution contains the average lifetime of the metastable dication and this information can be easily extracted by using a simple first order kinetic law. However, in this analysis is important to separate the portions of the plot referring to different sectors of the TOFMS: a simple $e^{-t/\tau}$ function applies only in the free field region of the drift tube, as discussed and indicated in Section 3. In the present case a result of lifetime τ of the order of magnitude of the μs is obtained. Following the discussion by Field and Eland [18], one has to consider that CO_2 is a particular case, because when the CO_2^{2+} dication is formed in a metastable state, the spread of lifetimes is large due to a manifold of vibro-electronic states, formed in the photoionization and leading to the opening of several different dissociation channels. Therefore, the measurements evidently yield average values of τ which depend on the time window over which the observations have been made [13,18] and also on the method used for the analysis of data. Actually, these different methods can attribute different weights to the several possible channels and to the regions of the ion path where dissociation can occur.

One has to emphasize that the distributions in Fig. 7, panels from (a) to (e), must not be confused with the experimental ones, because they are the distributions generated by the procedure, in order to minimize the chi-square of the coincidence plot data in the simulation. The KER distribution, that has been measured separately in the experiment [13,14], although larger, exhibits very similar most probable value. Also the lifetime extracted here is of the same order of magnitude of the one obtained [13] exploiting different methodologies of analysis.

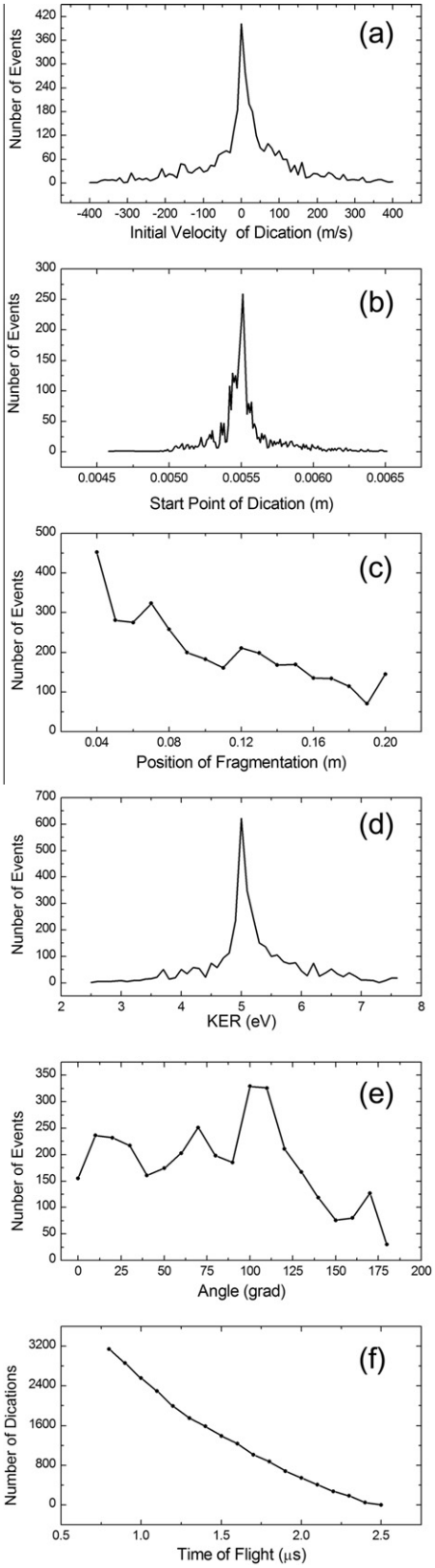

Fig. 7. Dynamical features extracted by the simulation trajectories on the CO_2^{2+} dication. Number of events observed in the simulation as a function of the variables. Panel (a): initial velocity. Panel (b): start point. Panel (c): position where dissociation occurs, along the drift tube. Panel (d): kinetic energy release (KER) of the two fragments. Panel (e): angular distribution of the fragment ions. Panel (f): number of dications along the ion flight path.

We expect that the methodology presented here can be used, with further improvements, for the analysis of many other systems, like the double photoionization of N_2O [11,12], and of benzene molecules [38] that we have recently investigated. Moreover the same methodology, appropriately extended and modified, could be used also for the analysis of angular distribution of products [12].

Acknowledgments

Financial contributions from the MIUR (Ministero dell'Istruzione, dell'Università e della Ricerca) are gratefully acknowledged. We acknowledge some travel supports by the "Sincrotrone Trieste S.C.p.A.". We wish to thank the "Fondazione Cassa di Risparmio di Perugia" for a financial support. Part of this project has been supported by the Brazilian Ministry of Education and KCM is grateful and wish to thank the CAPES for this grant.

Appendix Main. steps of the TOFMS-GSA algorithm

The whole TOFMS-GSA algorithm for mapping and searching the global minimum of the objective function f follows the steps:

1. Fix the q_A, q_V, and q_T parameters relative to the acceptance and visitation probability-distributions and to the temperature function, respectively.
2. Start, at first, the iterative process with an arbitrary initial guess vector of parameters $\vec{P} = (E_{KER}, \tau, v_o, S_o, \theta)$ and an high enough value for the "temperature" $T_{q_T}(n)$ at the GSA loop n.
3. Calculate the objective initial function $f(\vec{P}_n)$ using Eq. (1).
4. Calculate a new "temperature" in the GSA loop $n+1$ as

$$T_{q_{T_{n+1}}} = T_0 \frac{2^{q_T-1}-1}{(1+(n+1))^{q_T-1}-1}$$

where T_0 is the initial temperature.

5. Next, using the visiting probability distribution $g_{q_V}(T_{q_{T_{n+1}}}, x)$ as defined in Eq. (7) we calculate the new set of parameters

$$\vec{P}_{n+1} = (E_{KER_{n+1}}, t_{o_{n+1}}, v_{o_{n+1}}, S_{o_{n+1}}, \theta_{n+1}) = (E_{KER_n}, t_n, v_{o_n}, S_{o_n}, \theta_n) + \Delta(E_{KER_n}, t_n, v_{o_n}, S_{o_n}, \theta_n)$$

where $\Delta(E_{KER_n}, t_n, v_{o_n}, S_{o_n}, \theta_n) = (g(x_K), g(x_t), g(x_v), g(x_S), g(x_\theta))$ and $x_i \in [0,1]$ is a random number.

6. At the GSA step $n+1$ and using these new set of parameters over the Newton's equations, we calculate, in sector k, the following physical properties:

(a) for the dication with charge q_D

$d_{(k=1)_{n+1}} = S_{o_{n+1}}$	initial position in sector $k=1$, generated by GSA
$d_{(k>1)_{n+1}} =$ constant	dication traveled distance or dimension of sector k
$a_{D_{k_{n+1}}} = \frac{q_D}{M_D}\frac{V_k - V_{k-1}}{d_{k_{n+1}}}$	acceleration on the GSA step $n+1$
$t_{D_{k_{n+1}}} = t_{o_{n+1}}$	initial time of flight in sector $k=1$, generated by GSA
$t_{D_{k_{n+1}}} = \frac{-v_{D_{(k-1)_{n+1}}} + \sqrt{v^2_{D_{(k-1)_{n+1}}} + 2d_{k_{n+1}} a_{D_{k_{n+1}}}}}{a_{D_{k_{n+1}}}}$	Time of flight in the sector k
$t_{T_k} = \sum_{i=1}^{k} t_{Di}$	dication total time of flight until the fragmentation
$v_{D_{k=1}} = v_{o_{n+1}}$	initial velocity in sector $k=1$, generated in the $n+1$ GSA step
$v_{D_{k_{n+1}}} = v_{D_{(k-1)_{n+1}}} + a_{D_{(k+1)_{n+1}}} t_{D_{(k+1)_{n+1}}}$	dication velocity at the final of sector k
$S_{D_k} = S_{o_{n+1}} + \sum_{i>1}^{k} d_i$	dication total distance traveled until the fragmentation in sector k

(b) for the ion or fragment $i = A, B$ we used the following motions equations

τ	fragmentation time, generated by GSA
$\Delta S_{k_{n+1}} = d_{k_{n+1}} - v_{D_{k_{n+1}}}(\tau - t_{T_{k-1}}) - \frac{1}{2} a_{D_{k_{n+1}}} (\tau - t_{T_{k-1}})^2$	dication total distance traveled in sector k
$a_{i_{k_{n+1}}} = \frac{q_i}{M_i}\frac{V_k - V_{k-1}}{\Delta d_{k_{n+1}}}$	fragment acceleration
$t_{i_{k_{n+1}}} = \frac{-v_{i_{(k-1)_{n+1}}} + \sqrt{v^2_{i_{(k-1)_{n+1}}} + 2\Delta S_{k_{n+1}} a_{i_{k_{n+1}}}}}{a_{i_{k_{n+1}}}}$	time of flight of ion i in the sector k
$v_{z_A} = \sqrt{\frac{E_{KER}}{M_A\left(1+\frac{M_A}{M_B}\right)}}\cos(\theta)$	z component of the velocity of the fragment A
$v_{z_B} = \sqrt{\frac{E_{KER}}{M_B\left(1+\frac{M_B}{M_A}\right)}}\cos(\theta - \pi)$	z component of the velocity of the fragment B
$v_{i_{k_{n+1}}} = v_{D_{k_{n+1}}} + v_{i_{(k-1)_{n+1}}} + a_{i_{k_{n+1}}} t_{i_{k_{n+1}}}$	velocity of ion i in the sector k

It is important to take into account that, in the sector 3, the electrical field and the ions acceleration are zero.

1. Calculate, at the time $n+1$, the new objective function

$f(\vec{P}_{n+1}) = f(E_{KER_{n+1}}, t_{o_{n+1}}, v_{o_{n+1}}, S_{o_{n+1}}, \theta_{n+1})$ using Eq. (1). The new function value will be accepted or not according to the rule: if $f(\vec{P}_{n+1}) \leqslant f(\vec{P}_n)$ replace P_n by P_{n+1}, if $f(\vec{P}_{n+1}) > f(\vec{P}_n)$ run a random number $r \in [0,1]$, if $r > A_{acc}$, the acceptance probability defined in Eq. (9), retain $\vec{P}_{n+1}$, otherwise, replace $\vec{P}_n$ by $\vec{P}_{n+1}$.

1. Take $n \to n+1$ and return to step (3) until the convergence of $f(\vec{P}_n)$ is reached within the desired convergence criterion.

The steps can be described by the following flowchart:

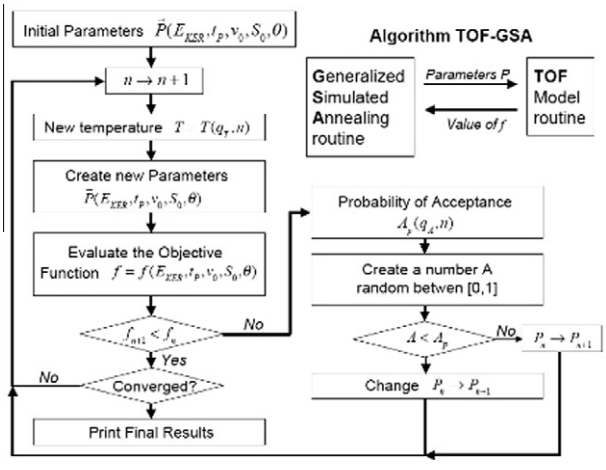

In its original form [28], GSA was defined with two independent parameters q_A and q_V, used in the definition of the following functions: acceptance probability $A_{acc}(q_A)$, visiting distribution g_{q_V} and temperature T_{q_V}. In our case the objective function is defined in terms of time of flight of ionic fragments.

References

[1] L. Pauling, J. Chem. Phys. 1 (1933) 56.
[2] S.G. Cox, A.D.J. Critchley, P.S. Kreynin, I.R. McNab, R.C. Shiellx, F.E. Smith, Phys. Chem. Chem. Phys. 5 (2003) 663.
[3] M. Moix-Teixidor, F. Pirani, P. Candori, S. Falcinelli, F. Vecchiocattivi, Chem. Phys. Lett. 379 (2003) 139.
[4] P. Candori, S. Falcinelli, F. Pirani, F. Tarantelli, F. Vecchiocattivi, Chem. Phys. Lett. 436 (2007) 322.
[5] M. Alagia, B.G. Brunetti, P. Candori, S. Falcinelli, M. Moix-Teixidor, F. Pirani, R. Richter, S. Stranges, F. Vecchiocattivi, J. Chem. Phys. 120 (2004) 6985.
[6] S.S. Prasad, D.R. Furman, J. Geophys. Res. 80 (1975) 1360.
[7] S.D. Rosner, R. Cameron, T.J. Scholl, R.A. Holt, J. Mol. Spectrosc. 189 (1998) 83.
[8] M. Alagia, F. Biondini, B.G. Brunetti, P. Candori, S. Falcinelli, M. Moix-Teixidor, F. Pirani, R. Richter, S. Stranges, F. Vecchiocattivi, J. Chem. Phys. 121 (2004) 10508.
[9] M. Alagia, M. Boustimi, B.G. Brunetti, P. Candori, S. Falcinelli, R. Richter, S. Stranges, F. Vecchiocattivi, J. Chem. Phys. 117 (2002) 1098.
[10] M. Alagia, B.G. Brunetti, P. Candori, S. Falcinelli, M. Moix Teixidor, F. Pirani, R. Richter, S. Stranges, F. Vecchiocattivi, J. Chem. Phys. 124 (2006) 204318.
[11] M. Alagia, P. Candori, S. Falcinelli, M. Lavollée, F. Pirani, R. Richter, S. Stranges, F. Vecchiocattivi, Chem. Phys. Lett. 432 (2006) 398.
[12] M. Alagia, P. Candori, S. Falcinelli, M. Lavollée, F. Pirani, R. Richter, S. Stranges, F. Vecchiocattivi, J. Chem. Phys. 126 (2007) 201101.
[13] M. Alagia, P. Candori, S. Falcinelli, M. Lavollée, F. Pirani, R. Richter, S. Stranges, F. Vecchiocattivi, J. Phys. Chem. A 113 (2009) 14755.
[14] M. Alagia, P. Candori, S. Falcinelli, M. Lavolleé, F. Pirani, R. Richter, S. Stranges, F. Vecchiocattivi, Phys. Chem. Chem. Phys. 12 (2010) 5389.
[15] M. Alagia, P. Candori, S. Falcinelli, F. Pirani, M.S. Pedrosa Mundim, R. Richter, M. Rosi, S. Stranges, F. Vecchiocattivi, Phys. Chem. Chem. Phys. (2011), doi:10.1039/C0CP02678F.
[16] M. Alagia, B.G. Brunetti, P. Candori, S. Falcinelli, M. Moix-Teixidor, F. Pirani, R. Richter, S. Stranges, F. Vecchiocattivi, J. Chem. Phys. 120 (2004) 6980.
[17] S. Hsieh, J.H.D. Eland, J. Phys. B: At. Mol. Opt. Phys. 30 (1997) 4515.
[18] T.A. Field, J.H.D. Eland, Chem. Phys. Lett. 211 (1993) 436.
[19] A.E. Slattery, T.sA. Field, M. Ahmad, R.I. Hall, J. Lambourne, F. Penent, P. Lablanquie, J.H.D. Eland, J. Chem. Phys. 122 (2005) 084317.
[20] M. Lavollée, Rev. Sci. Instrum. 70 (1999) 2968.
[21] W. Wiley, I. Mclaren, Rev. Sci. Instr. 26 (1955) 1150.
[22] M.A. Moret, P.M. Bisch, K.C. Mundim, P.G. Pascutti, Biophys. J. 82 (2002) 1123.
[23] S. Kirkpatrick, C. Gelatt, M. Vecchi, Science 220 (1983) 671.
[24] S. Kirkpatrick, J. Stat. Phys. 34 (1984) 975.
[25] N. Metropolis, S. Ulam, J. Am. Stat. Assoc. 44 (1949) 335.
[26] S. Geman, D. Geman, IEEE Trans. Pattern Anal. Mach. Intell. 6 (1984) 721.
[27] H. Szu, R. Hartley, Phys. Lett. A 122 (1987) 157.
[28] K.C. Mundim, C. Tsallis, Int. J. Quant. Chem. 58 (1996) 373.
[29] C. Tsallis, D. Stariolo, Physica A 233 (1996) 395.
[30] A.F.A. Vilela, J.J.S. Neto, K.C. Mundim, M.S.P. Mundim, R. Gargano, Chem. Phys. Lett. 359 (2002) 420.
[31] C.S. Esteves, H.C.B. de Oliveira, L. Ribeiro, R. Gargano, K.C. Mundim, Chem. Phys. Lett. 427 (2006) 10.
[32] K.C. Mundim, T.J. Lemaire, A. Bassrei, Physica A 252 (1998) 405.
[33] D.E. Ellis, K.C. Mundim, D. Fuks, S. Dorfman, A. Berner, Mat. Sci. Semicond. Proc. 3 (2000) 123.
[34] S. Dorfman, D. Fuks, L.A.C. Malbouisson, K.C. Mundim, Comput. Mat. Sci. 27 (2003) 199.
[35] H.C.B. de Oliveira, C.S. Esteves, R. Gargano, M.A. Chaer do Nascimento, L.A.C. Malbouisson, K.C. Mundim, Int. J. Quant. Chem. 108 (2008) 2540.
[36] M.D. de Andrade, K.C. Mundim, L.A.C. Malbouisson, Int. J. Quant. Chem. 103 (2005) 493.
[37] A. Dall'Igna, R. Silva, K.C. Mundim, L. Dardenne, Gen. Mol. Biol. 27 (2004) 616.
[38] M. Alagia, P. Candori, S. Falcinelli, F. Pirani, M. S. P. Mundim, R. Richter, M. Rosi, S. Stranges, F. Vecchiocattivi (in preparation).